

# Neural ODE and DAE Modules for Power System Dynamic Component Modeling

Tannan Xiao, *IEEE Member*, Ying Chen, *IEEE Member*, Tirui He, and Huizhe Guan

**Abstract**—The time-domain simulation is fundamental for power system transient stability analysis. Accurate and reliable simulations depend on accurate dynamic component modeling. In practical power systems, dynamic component modeling has long faced the challenges of model determination and model calibration, especially with the rapid development of renewable generation and power electronics. In this paper, based on the general framework of neural ordinary differential equations (ODEs), a modified neural ODE module and a neural differential-algebraic equations (DAEs) module for power system dynamic component modeling are proposed. Autoencoder-based frameworks of the proposed modules are put forward to upgrade model performance. The methodology of integrating neural dynamic models trained by the proposed neural modules into transient stability simulations is demonstrated. With datasets consisting of sampled curves of input variables and output variables, the proposed modules can be used to fulfill the tasks of black-box modeling, physics-data-integrated modeling, parameter inference, etc. Tests are carried out in the IEEE-39 system to prove the validity and potentiality of the proposed modules.

**Index Terms**—Power system dynamics, power system simulations, dynamic modeling, ordinary differential equations, differential-algebraic equations, neural networks, autoencoder

## I. INTRODUCTION

FROM the perspective of power systems, ensuring the normal and healthy functioning of components and the stable operation of the system is a crucial task. The success of this task relies heavily on accurate dynamic component modeling and power system dynamic simulations [1].

Power system dynamic component modeling is already a mature and generally researched area [2]. Practical power systems have long faced the challenges of model determination and model calibration, especially with the rapid development of renewable generation and power electronics. On the one hand, the physics of some components is still under research. We may not have enough prior knowledge to construct or select a proper model, e.g., the equivalent dynamic modeling of a wind farm considering low voltage ride-through. The measurable variables might also be limited, which means only partial dynamics is observable. On the other hand, the dynamic models of some new devices, e.g., a new type of regulator, may be completely black boxes due to the confidential protocols of the equipment companies. The only accessible knowledge is the settings and measured curves of the input and output variables of the equipment. Although a dynamic link library (DLL) file of the equipment is usually available for specific kinds of dynamic

simulations, it is hard to learn the inner mechanism and optimize the control schemes of the device. The DLL file may also seriously degrade the efficiency of the simulation program and affect the gradient calculation process for stability control. In these situations, model determination and model calibration should be done simultaneously with very limited or even no prior knowledge except the input and output settings and sampled curves.

These challenges are the reason why these topics have been well studied and researchers are still pursuing research on them.

### A. Related Works

As for the model determination problem, intuitively, dynamic components such as generating units, loads, regulators, etc., can be modeled based on their physics. It is the traditional and inevitable way of obtaining an accurate dynamic model that can be used in power system simulations. There have been continuing studies down this path and many physics-based models have been proposed, e.g., 2<sup>nd</sup>-order to 6<sup>th</sup>-order generator models [3], the induction motor model [3], generic models for wind turbines [4], the single diode solar cell model [5], the battery energy storage system model in the d-q axes [6], the average-value model of high-speed response brushless excitation systems [7], the IEEE G1 governor model [8], the multi-band power system stabilizer [9], etc. On the other hand, from the point of view of transmission networks, feeders in the substations, networked microgrids, traditional distribution networks, and active distribution networks (ADNs) containing distributed energy resources will usually be modeled as an equivalent dynamic load. A comprehensive review of load modeling can be found in [10]. The load model is usually selected by the operators based on their experience and the dynamic characteristics of the components in the network. Therefore, the load modeling of practical power systems often shows regional characteristics [2].

As for the model calibration problem, the most traditional way is to design physics-based field tests and directly calculate the parameters by obtaining needed measurements. Various measurement-based model calibration methods, which are essentially a posterior optimization approach, have been proposed. A weighted least-square estimation algorithm that obtains the maximum likelihood estimation of the parameters is presented in [11]. Optimization-based methods formulate the parameter estimation problem as an optimization problem and solve it using gradient-based algorithms [12], trajectory sensitivity-based algorithms [13], [14], and meta-heuristic algorithms [15]. Kalman filter-based methods calibrate the parameters by representing the probability density function of the augmented state variables [16], [17]. Bayesian inference-based algorithms optimize the parameters by minimizing the errors of approximate posteriors [18], [19].

Research on machine learning (ML) has achieved a growth spurt in the past few years. ML algorithms have been applied to a variety of power system studies including dynamic component modeling. Reinforcement learning algorithms [20] calibrate model parameters

This paper is first submitted to IEEE. This work was supported in part by the National Natural Science Foundation of China (NSFC) under the Project No. 52107104, (Corresponding Author: Ying Chen).

All the authors are with the Department of Electrical Engineering, Tsinghua University, Beijing, 100084, China (Email: [cexiaoxh@gmail.com](mailto:cexiaoxh@gmail.com), [chen\\_ying@tsinghua.edu.cn](mailto:chen_ying@tsinghua.edu.cn), [hetirui@qq.com](mailto:hetirui@qq.com), [mark.mghz@gmail.com](mailto:mark.mghz@gmail.com)).

by establishing an agent-environment interactive mechanism. Deep learning algorithms are used for the equivalent modeling of ADNs [21], model calibration [22], or to identify Koopman eigenfunctions for linear representation of nonlinear systems [23], etc. Neural ordinary differential equations (ODEs) proposed in [24] have been used to establish neural models of networked microgrids for reachability analysis [25]. The framework of neural ODE has drawn a lot of attention. Compared with other methods, the framework of neural ODE keeps the numerical integration structure, which is a very important prior knowledge. The framework has inspired many physics-data-integrated studies such as neural partial differential equations [26], the Hamilton neural networks [27], the Lagrangian neural networks [28], etc. These studies have demonstrated the great potential of neural ODE in solving the dynamics of physical systems.

### B. Contributions

In this paper, we try to deal with the challenges of power system component dynamic modeling with a data-driven approach. The applications of neural ODE [24] for power system dynamic component modeling and transient stability simulations are discussed and tested. The contributions of this paper are as follows.

1) For power system dynamic component modeling, a modified neural ODE module and a neural differential-algebraic equations (DAE) module for power system dynamic component modeling are proposed. Autoencoder-based frameworks are presented to improve the flexibility and performance of the proposed neural modules.

2) Considering initial value calculation, discrete event handling, and convergence maintenance, the methodology of integrating neural dynamic models trained by the proposed neural modules into transient stability simulations is demonstrated.

3) Under the scenarios of black-box modeling, physics-data-integrated modeling, and model calibration, the proposed neural modules are implemented with Python and made public on GitHub ([https://github.com/xxh0523/Py\\_PSNODE](https://github.com/xxh0523/Py_PSNODE)). The trained models are integrated into a transient stability simulator and tested in the IEEE-39 system.

### C. Paper Organization

The remainder of the papers is as follows. Section II introduces the problem formulation of power system dynamic component modeling. The modified neural ODE module and neural DAE module are illustrated in Section III. In section IV, how to integrate the neural models into transient stability simulations is demonstrated. Two simple but representative cases of an excitation controller and a classic synchronous machine are designed and tested in Section V and Section VI. Discussions on the proposed neural modules are carried out in Section VII. Conclusions are drawn in Section VIII.

## II. PROBLEM FORMULATION

As mentioned before, the target of this paper is to build a mathematical model of dynamic components in a data-driven manner and integrate that model into transient stability simulations, as shown in Fig. 1. The neural modules proposed in this paper are used to build dynamic models and the learned models are integrated into simulations.

### A. Data-Driven Dynamic Component Modeling

In power system transient stability simulations, the dynamic components can be divided into two types according to whether the component produces injection currents into the power network. For

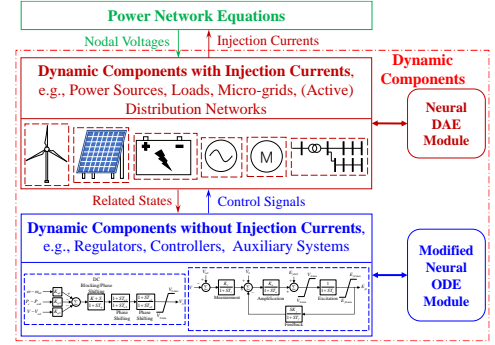


Fig. 1. Overview of dynamic component modeling and proposed neural modules.

the ones that do not produce injection currents, e.g., an excitation controller, the dynamics can be formulated as:

$$\dot{\mathbf{x}} = \mathbf{f}(\mathbf{x}, \mathbf{z}) \quad (1)$$

where  $\mathbf{x}$  is the state vector of the component whose time derivatives are equal to  $\mathbf{f}(\mathbf{x}, \mathbf{z})$ , and  $\mathbf{z}$  is the vector of required external variables. Taking an exciter as an example, in addition to the state variables, the nodal voltage of the generator-connected bus is needed for calculating derivatives, i.e., the nodal voltage belongs to  $\mathbf{z}$ .

For the components that produce injection currents into the power network, the dynamics can be formulated as:

$$\dot{\mathbf{x}} = \mathbf{f}(\mathbf{x}, \mathbf{i}, \mathbf{v}, \mathbf{z}) \quad (2)$$

$$\mathbf{i} = \mathbf{g}(\mathbf{x}, \mathbf{v}, \mathbf{z}) \quad (3)$$

where  $\mathbf{i}$  is the injection current,  $\mathbf{v}$  is the nodal voltage of the component-connected bus, and  $\mathbf{g}$  is the function of injection current calculation. Taking a synchronous machine as an example, the inner electric potentials, rotor angle, rotor speed, and state variables of regulators belong to  $\mathbf{x}$ , the active and reactive power at the starting instant and at the current step may belong to  $\mathbf{z}$ .

Accordingly, the model determination process is to properly set  $\mathbf{x}$  and  $\mathbf{z}$ , then determine functions  $\mathbf{f}$  and  $\mathbf{g}$ . The model calibration process is to estimate the parameters in functions  $\mathbf{f}$  and  $\mathbf{g}$  based on field tests or sampled curves. In this paper, we are trying to model dynamic components in a data-driven manner. A dataset of all or part of the relative variables shown in (4) are sampled:

$$\mathcal{S} = \{\hat{\mathbf{x}}, \hat{\mathbf{i}}, \hat{\mathbf{v}}, \hat{\mathbf{z}}\} \quad (4)$$

where  $\mathcal{S}$  denotes the dataset, and  $\hat{\mathbf{x}}$ ,  $\hat{\mathbf{i}}$ ,  $\hat{\mathbf{v}}$ , and  $\hat{\mathbf{z}}$  contains the ground-truth values of  $\mathbf{x}$ ,  $\mathbf{i}$ ,  $\mathbf{v}$ , and  $\mathbf{z}$ , respectively. Based on this dataset, a posterior model and its parameters need to be determined.

### B. Data-driven Model-Integrated Dynamic Simulations

In transient stability simulations, the overall dynamics of a power system can be modeled as a group of high-dimensional non-linear DAEs including ODEs (5) for all the dynamic devices and algebraic equations (AEs) (6) for the power network:

$$\dot{\mathbf{x}} = \mathbf{f}(\mathbf{x}, \mathbf{V}) \quad (5)$$

$$\mathbf{G}(\mathbf{x}, \mathbf{V}) = \mathbf{YV} - \mathbf{I}(\mathbf{x}, \mathbf{V}) = \mathbf{0} \quad (6)$$

where  $\mathbf{x}$  is the state vector of the system, whose time derivatives are equal to  $\mathbf{f}(\mathbf{x}, \mathbf{V})$ ,  $\mathbf{V}$  is the bus voltage vector,  $\mathbf{I}$  is the injection current vector,  $\mathbf{Y}$  is the admittance matrix, and  $\mathbf{G}$  represents the whole network equations. The system DAEs can be solved with the simultaneous approach or the alternating approach [3]. It is obvious that the ODE models shown in (1) and DAE models shown in (2) and (3) can be easily integrated into the system DAEs shown in (5) and (6). It should also be easy to integrate the dynamic models built by the data-driven approach into simulations as well. The integration should not greatly affect the solution procedures.

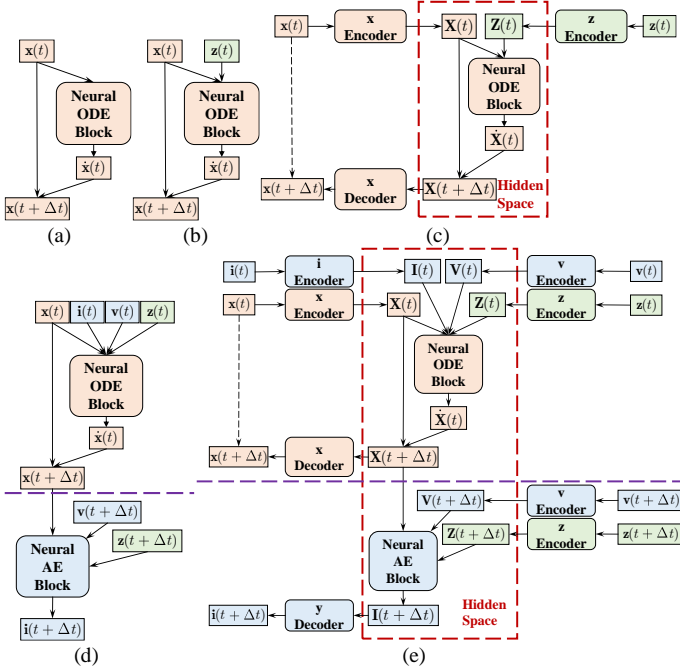


Fig. 2. Structures of (a) original neural ODE module, (b) modified neural ODE module, (c) autoencoder-based modified neural ODE module, (d) neural DAE module, and (e) autoencoder-based neural DAE module.

### III. MODIFIED NEURAL ODE MODULE AND NEURAL DAE MODULE FOR POWER SYSTEM DYNAMIC COMPONENT MODELING

#### A. General Framework of Neural ODE

The structure of the original Neural ODE module, as shown in Fig. 2(a), was first proposed by Chen *et al* in 2018 [24]. A neural ODE block consisting of neural networks is used to formulate a parameterized derivative function, as shown in (7):

$$\mathbf{f}_\theta(\mathbf{x}; \theta) \doteq \dot{\mathbf{x}} = \mathbf{f}(\mathbf{x}) \quad (7)$$

where  $\theta$  denotes parameters of the neural ODE block. Given the initial values  $\mathbf{x}(0)$ , the integration step  $\Delta t$ , the integration time  $T$ , and the derivative function (7), a series of  $\mathbf{x}$  can be easily calculated with a numerical integration method. For the convenience of demonstration, all the modules displayed in Fig. 2 use the Euler method as an example and the stepwise integration is as follows:

$$\mathbf{x}(t + \Delta t) = \mathbf{x}(t) + \Delta t \cdot \mathbf{f}(\mathbf{x}(t)) \quad (8)$$

The neural ODE block can be trained with a data set of sampled curves of  $\mathbf{x}$ . In (9), a loss function  $\mathcal{L}$  is defined to optimize  $\theta$ :

$$\begin{aligned} \theta &= \arg \min_{\theta} \sum_{i=1}^N \mathcal{L}(\mathbf{x}_i, \hat{\mathbf{x}}_i; \theta) \\ \text{s.t. } \dot{\mathbf{x}}_i &= \mathbf{f}_\theta(\mathbf{x}_i; \theta), \mathbf{x}_i(0) = \hat{\mathbf{x}}_i(0), t \in [0, T] \\ \dot{\hat{\mathbf{x}}}_i &= \mathbf{f}(\hat{\mathbf{x}}_i), \hat{\mathbf{x}}_i(0) = \hat{\mathbf{x}}_i(0), t \in [0, T] \\ \mathcal{S} &= \{\hat{\mathbf{x}}_i\}, i = 1, 2, \dots, N \end{aligned} \quad (9)$$

where  $N$  denotes the number of samples in the training set,  $\mathbf{x}$  denotes the series of state variables predicted using the neural ODE module,  $\mathcal{S}$  denotes the sampled dataset, and  $\hat{\mathbf{x}}$  denotes the ground-truth series. As can be seen, with the same input  $\hat{\mathbf{x}}_i(0)$ ,  $\mathbf{x}_i$  and series  $\hat{\mathbf{x}}_i$  can be obtained with numerical integration.

To optimize  $\theta$ , the adjoint sensitivity method [29], which is also introduced in [24] and [25], can be adopted. By forming a Hamiltonian  $\mathcal{H}$  [30], as shown in (10), the gradients with respect to  $\theta$  can be calculated with a backward integration as shown in (11):

$$\mathcal{H}(\mathbf{x}; \theta, \lambda) = \lambda^T \mathbf{f}_\theta(\mathbf{x}; \theta) \quad (10)$$

$$\nabla_{\theta} \mathcal{L} = \frac{\partial \mathcal{L}}{\partial \theta} = \int_{\tau}^0 \frac{\partial \mathcal{H}}{\partial \theta} dt = \int_{\tau}^0 \lambda^T \frac{\partial \mathbf{f}_{\theta}}{\partial \theta} dt \quad (11)$$

where  $\lambda$  denotes the Lagrange multiplier, the time derivatives of  $\lambda$  obey (12), and  $\lambda(T)$  obeys (13):

$$\dot{\lambda} = -\frac{\partial \mathcal{H}}{\partial \mathbf{x}} = -\lambda^T \frac{\partial \mathbf{f}_{\theta}}{\partial \mathbf{x}} \quad (12)$$

$$\lambda(T) = \frac{\partial \mathcal{L}}{\partial \mathbf{x}(T)} \quad (13)$$

Like the forward integration, a numerical integration method can be used to solve the backward integration using a negative integration step  $-\Delta t$ . The parameters can be easily optimized after the gradients  $\nabla_{\theta} \mathcal{L}$  are obtained, e.g., by applying the stochastic gradient descent (SGD) method or the Adam optimizer [31].

#### B. Proposed Modified Neural ODE Module

Based on the general framework of neural ODE, for the components shown in (1) that do not produce injection currents into the power network, the dynamics of the component and the neural derivative function can be formulated as (14):

$$\mathbf{f}_{\theta}(\mathbf{x}, \mathbf{z}; \theta) \doteq \dot{\mathbf{x}} = \mathbf{f}(\mathbf{x}, \mathbf{z}) \quad (14)$$

Accordingly, a modified neural ODE module is shown in Fig. 2(b). An equality constraint is added to (9) and the overall optimization is formulated as:

$$\begin{aligned} \theta &= \arg \min_{\theta} \sum_{i=1}^N \mathcal{L}(\mathbf{x}_i, \hat{\mathbf{x}}_i; \theta) \\ \text{s.t. } \dot{\mathbf{x}}_i &= \mathbf{f}_{\theta}(\mathbf{x}_i, \hat{\mathbf{z}}_i; \theta), \mathbf{x}_i(0) = \hat{\mathbf{x}}_i(0), t \in [0, T] \\ \dot{\hat{\mathbf{x}}}_i &= \mathbf{f}(\hat{\mathbf{x}}_i, \hat{\mathbf{z}}_i), \hat{\mathbf{x}}_i(0) = \hat{\mathbf{x}}_i(0), t \in [0, T] \\ \mathcal{S} &= \{\hat{\mathbf{x}}_i, \hat{\mathbf{z}}_i\}, i = 1, 2, \dots, N \end{aligned} \quad (15)$$

where  $\hat{\mathbf{z}}$  denotes the ground-truth values of  $\mathbf{z}$ . After applying the adjoint sensitivity method, parameters  $\theta$  can be optimized based on (10)-(13) by changing  $\mathbf{f}_{\theta}(\mathbf{x}; \theta)$  to  $\mathbf{f}_{\theta}(\mathbf{x}, \mathbf{z}; \theta)$ .

#### C. Proposed Neural DAE Module

For the components shown in (2) and (3) that produce injection currents into the power network, a more complex module illustrated in Fig. 2(d) is designed by adding a neural AE block. The dynamics can be approximated using the neural DAE module as follows:

$$\mathbf{f}_{\theta}(\mathbf{x}, \mathbf{i}, \mathbf{v}, \mathbf{z}; \theta) \doteq \dot{\mathbf{x}} = \mathbf{f}(\mathbf{x}, \mathbf{i}, \mathbf{v}, \mathbf{z}) \quad (16)$$

$$\begin{aligned} \mathbf{G}_{\xi}(\mathbf{x}, \mathbf{i}, \mathbf{v}, \mathbf{z}; \xi) &= \mathbf{i} - \mathbf{g}_{\xi}(\mathbf{x}, \mathbf{v}, \mathbf{z}; \xi) = \mathbf{0} \\ &= \mathbf{G}(\mathbf{x}, \mathbf{i}, \mathbf{v}, \mathbf{z}) = \mathbf{i} - \mathbf{g}(\mathbf{x}, \mathbf{v}, \mathbf{z}) \end{aligned} \quad (17)$$

where  $\mathbf{G}_{\xi}$  denotes the neural AEs,  $\mathbf{g}_{\xi}$  denotes the neural AE block,  $\xi$  is the parameters of the neural AE block.

Similarly, the optimization of  $\theta$  and  $\xi$  can be formulated, as shown in (18).

$$\begin{aligned} \theta, \xi &= \arg \min_{\theta, \xi} \sum_{i=1}^N \mathcal{L}(\mathbf{x}_i, \hat{\mathbf{x}}_i, \hat{\mathbf{i}}_i, \hat{\mathbf{v}}_i; \theta, \xi) \\ \text{s.t. } \dot{\mathbf{x}}_i &= \mathbf{f}_{\theta}(\mathbf{x}_i, \hat{\mathbf{i}}_i, \hat{\mathbf{v}}_i, \hat{\mathbf{z}}_i; \theta) \\ \mathbf{G}_{\xi}(\mathbf{x}_i, \hat{\mathbf{i}}_i, \hat{\mathbf{v}}_i, \hat{\mathbf{z}}_i; \xi) &= \hat{\mathbf{i}}_i - \mathbf{g}_{\xi}(\mathbf{x}_i, \hat{\mathbf{v}}_i, \hat{\mathbf{z}}_i; \xi) = \mathbf{0} \\ \mathbf{x}_i(0) &= \hat{\mathbf{x}}_i(0), \hat{\mathbf{i}}_i(0) = \hat{\mathbf{i}}_i(0), t \in [0, T] \\ \dot{\hat{\mathbf{x}}}_i &= \mathbf{f}(\hat{\mathbf{x}}_i, \hat{\mathbf{i}}_i, \hat{\mathbf{v}}_i, \hat{\mathbf{z}}_i) \\ \mathbf{G}(\hat{\mathbf{x}}_i, \hat{\mathbf{i}}_i, \hat{\mathbf{v}}_i, \hat{\mathbf{z}}_i) &= \hat{\mathbf{i}}_i - \mathbf{g}(\hat{\mathbf{x}}_i, \hat{\mathbf{v}}_i, \hat{\mathbf{z}}_i) = \mathbf{0} \\ \hat{\mathbf{x}}_i(0) &= \hat{\mathbf{x}}_i(0), \hat{\mathbf{i}}_i(0) = \hat{\mathbf{i}}_i(0), t \in [0, T] \\ \mathcal{S} &= \{\hat{\mathbf{x}}_i, \hat{\mathbf{i}}_i, \hat{\mathbf{v}}_i, \hat{\mathbf{z}}_i\}, i = 1, 2, \dots, N \end{aligned} \quad (18)$$

The adjoint sensitivity method can also be used to derive gradients with respect to  $\theta$  and  $\xi$ , which has the same form as the trajectory sensitivity method in the research field of power systems. The Hamiltonian  $\mathcal{H}$  is defined in (19) and the gradients can be calculated as shown in (20) and (21):

$$\mathcal{H}(\mathbf{x}, \mathbf{i}, \mathbf{v}, \mathbf{z}; \theta, \xi, \lambda, \beta) = \lambda^T \mathbf{f}_\theta(\mathbf{x}, \mathbf{i}, \mathbf{v}, \mathbf{z}; \theta) + \beta^T \mathbf{G}_\xi(\mathbf{x}, \mathbf{i}, \mathbf{v}, \mathbf{z}; \xi) \quad (19)$$

$$\begin{aligned} \nabla_\theta \mathcal{L} &= \frac{\partial \mathcal{L}}{\partial \theta} = \int_T^0 \frac{\partial \mathcal{H}}{\partial \theta} dt = \int_T^0 \lambda^T \frac{\partial \mathbf{f}_\theta}{\partial \theta} + \beta^T \frac{\partial \mathbf{G}_\xi}{\partial \theta} dt \\ &= \int_T^0 \lambda^T \frac{\partial \mathbf{f}_\theta}{\partial \theta} + \beta^T \frac{\partial \mathbf{x}}{\partial \theta} \frac{\partial \mathbf{G}_\xi}{\partial \mathbf{x}} dt \end{aligned} \quad (20)$$

$$\nabla_\xi \mathcal{L} = \frac{\partial \mathcal{L}}{\partial \xi} = \int_T^0 \frac{\partial \mathcal{H}}{\partial \xi} dt = \int_T^0 \lambda^T \frac{\partial \mathbf{i}}{\partial \xi} \frac{\partial \mathbf{f}_\theta}{\partial \mathbf{i}} + \beta^T \frac{\partial \mathbf{G}_\xi}{\partial \xi} dt \quad (21)$$

where  $\lambda$  and  $\beta$  denote the Lagrange multipliers,  $\beta$  and the time derivatives of  $\lambda$  obey (22) and (23), and  $\lambda(T)$  obeys (24):

$$\dot{\lambda} = -\frac{\partial \mathcal{H}}{\partial \mathbf{x}} = -\lambda^T \frac{\partial \mathbf{f}_\theta}{\partial \mathbf{x}} - \beta^T \frac{\partial \mathbf{G}_\xi}{\partial \mathbf{x}} \quad (22)$$

$$\mathbf{0} = \frac{\partial \mathcal{H}}{\partial \mathbf{i}} = \lambda^T \frac{\partial \mathbf{f}_\theta}{\partial \mathbf{i}} + \beta^T \frac{\partial \mathbf{G}_\xi}{\partial \mathbf{i}} \quad (23)$$

$$\lambda(T) = \frac{\partial \mathcal{L}}{\partial \mathbf{x}(T)} \quad (24)$$

Similarly, we can derive gradients with respect to  $\theta$  and  $\xi$  using a backward numerical integration.

#### D. Autoencoder-based frameworks

Frameworks of autoencoder-based neural modules are put forward in Fig. 2. (c) and Fig. 2. (e). The reason for introducing these structures is that a difficult problem in the original space may change to a simpler one after a non-linear dimensionality transformation. These techniques have also been widely used in computer science [32] and physics-data-integrated physics modeling [23].

The autoencoder-based modules are flexible. In real-world power systems, dynamic components are not usually completely observable. Only a very limited number of state variables can be measured. In this situation, a dimensionality-raising autoencoder is recommended to learn an approximation of the unseen dynamics in the hidden space. On the other hand, in an equivalent modeling situation, there are too many state variables and a low-dimensional manifold usually exists [33]. In this case, a dimensionality-reduction autoencoder is suggested to focus on the key features of the original dynamics. Therefore, in this paper, autoencoders are used to change dimensionality and improve model performance.

It should be noted that the encoding process only performs once to transform the initial value of  $\mathbf{x}$  and  $\mathbf{i}$  into the hidden space, whereas the decoding process is performed at every integration step including the starting step. The frameworks displayed in Fig. 2. (c) and Fig. 2. (e) are adopted for the convenience of description and understanding. The autoencoder-based variable transformations are shown in (25) and (26):

$$\begin{cases} \mathbf{X}(0) = \text{encoder}_x(\mathbf{x}(0)), \mathbf{Z}(t) = \text{encoder}_z(\mathbf{z}(t)) \\ \mathbf{x}(t) = \text{decoder}_x(\mathbf{X}(t)) \end{cases} \quad (25)$$

$$\begin{cases} \mathbf{X}(0) = \text{encoder}_x(\mathbf{x}(0)), \mathbf{Z}(t) = \text{encoder}_z(\mathbf{z}(t)) \\ \mathbf{I}(0) = \text{encoder}_i(\mathbf{i}(0)), \mathbf{v}(t) = \text{encoder}_v(\mathbf{v}(t)) \\ \mathbf{x}(t) = \text{decoder}_x(\mathbf{X}(t)), \mathbf{i}(t) = \text{decoder}_i(\mathbf{I}(t)) \end{cases} \quad (26)$$

---

#### Pseudo-code 1: Training Procedures of Neural Modules

---

Input the total number of samples  $N$ , the integration step  $\Delta t$ , the simulation time  $T$ , the mini-batch size  $m$ , the number of training epochs  $E$ , evaluation interval  $\Delta E$ ;

Get the sampled dataset  $\mathcal{S}$  by simulations with simulation time  $T$  and fixed integration step  $\Delta t$ . Split the samples to form a training set and a testing set.

**for**  $i=1$  **to**  $E$  **do**

**for**  $j=1$  **to**  $N/m$  **do**

Sample a mini-batch of  $m$  samples from the training dataset.

Input the minibatch into the neural module, perform forward integration, and

get  $\mathbf{x}$  and  $\mathbf{i}$ .

Perform backward integration and get  $\nabla_\theta \mathcal{L}$  and  $\nabla_\xi \mathcal{L}$ .

Update  $\theta$  and  $\xi$  with the optimizer based on  $\nabla_\theta \mathcal{L}$  and  $\nabla_\xi \mathcal{L}$ .

**end for**

**if**  $i \bmod \Delta E$  **then**

Evaluate the neural module in the testing dataset.

**end if**

**end for**

---

where  $\mathbf{X}$ ,  $\mathbf{Z}$ ,  $\mathbf{V}$ , and  $\mathbf{I}$  are the state variables in hidden space. The numerical integration and the injection current calculation take place in the hidden space.

#### E. Loss Function and Training Procedures

For the convenience of demonstration, we take  $(\mathbf{x}, \mathbf{i}, \mathbf{v}, \mathbf{z})$  and the neural DAE module as the example to explain the loss function. The L2 norm (27) of the differences between the predicted curves and the ground-truth curves can be adopted.

$$\mathcal{L} = \mathbf{w}_x^T \|\mathbf{x} - \hat{\mathbf{x}}\|_2 + \mathbf{w}_i^T \|\mathbf{i} - \hat{\mathbf{i}}\|_2 \quad (27)$$

where  $\mathbf{w}$  denotes the weighting factors of different variables. As mentioned before, the SGD method or the Adam optimizer can be applied to train the neural modules. The training procedures are demonstrated in Pseudo-code 1.

### IV. NEURAL MODULE-INTEGRATED TRANSIENT STABILITY SIMULATIONS

#### A. Basics of Power System Transient Stability Simulations

The system DAEs shown in (5) and (6) can be solved by the simultaneous approach or by the alternating approach. In the simultaneous approach, after applying implicit numerical integration methods to ODEs, ODEs will transform into algebraic equations and can be solved simultaneously with (6) using the Newton method iteratively, as shown in (28)-(29):

$$\begin{bmatrix} \mathbf{F}(\mathbf{x}, \mathbf{V}) \\ \mathbf{G}(\mathbf{x}, \mathbf{V}) \end{bmatrix} = \begin{bmatrix} \mathbf{0} \\ \mathbf{0} \end{bmatrix} \quad (28)$$

$$\begin{bmatrix} \frac{\partial \mathbf{F}}{\partial \mathbf{x}} & \frac{\partial \mathbf{F}}{\partial \mathbf{V}} \\ \frac{\partial \mathbf{G}}{\partial \mathbf{x}} & \frac{\partial \mathbf{G}}{\partial \mathbf{V}} \end{bmatrix} \begin{bmatrix} \Delta \mathbf{x} \\ \Delta \mathbf{V} \end{bmatrix} = \begin{bmatrix} -\mathbf{F} \\ -\mathbf{G} \end{bmatrix} \quad (29)$$

where  $\mathbf{F}(\mathbf{x}, \mathbf{V})$  are the transformed algebraic equations of ODEs. Taking the implicit trapezoidal method as an example,  $\mathbf{F}(\mathbf{x}, \mathbf{V})$  is shown in (30).

$$\begin{aligned} \mathbf{F}(\mathbf{x}, \mathbf{V}, t) &= \mathbf{x}(t) - \\ &\left\{ \mathbf{x}(t - \Delta t) + \frac{1}{2} \Delta t [\mathbf{f}(\mathbf{x}(t)) + \mathbf{f}(\mathbf{x}(t - \Delta t))] \right\} \end{aligned} \quad (30)$$

On the other hand, in the alternating approach, the ODEs and AEs are solved separately. Fast solution techniques [34] can be used to

improve numerical stability and accelerate the solution processes. Firstly, given the state vector  $\mathbf{x}(t)$  and bus voltage vector  $\mathbf{V}(t)$  at instant  $t$ , estimate the initial value  $\mathbf{V}^{(0)}(t+\Delta t)$ , or simply let  $\mathbf{V}^{(0)}(t+\Delta t) = \mathbf{V}(t)$ . Secondly, solve (5) to obtain  $\mathbf{x}^{(0)}(t+\Delta t)$  using the numerical integration method with  $\mathbf{x} = \mathbf{x}(t)$  and  $\mathbf{V} = \mathbf{V}^{(0)}(t+\Delta t)$ . Third, solve (6) for  $\mathbf{V}^{(1)}(t+\Delta t)$  with  $\mathbf{x} = \mathbf{x}^{(0)}(t+\Delta t)$  and  $\mathbf{V} = \mathbf{V}^{(0)}(t+\Delta t)$ . Then solve (5) again with  $\mathbf{x} = \mathbf{x}^{(0)}(t+\Delta t)$  and  $\mathbf{V} = \mathbf{V}^{(1)}(t+\Delta t)$ . The above iteration is repeated until convergence is reached.

As can be seen, the simultaneous approach is more rigorous and the dynamic models must support the calculation of partial derivatives shown in (29). In contrast, the alternating approach will cause errors and might affect the simulation accuracy, but this approach does not require partial derivatives and is widely used in industry-grade simulation programs because of its programming flexibility and simplicity, reliability, and robustness [3].

The DLL files provided by the equipment company cannot provide derivative information in most cases. Therefore, they cannot be used in the simultaneous approach. On the other hand, a DLL-based black-box model can be easily integrated into the alternating approach-based simulations. However, the integration of a DLL-based model may still seriously affect the simulation efficiency, especially in a GPU-based simulator.

### B. Integrating Neural Models into Simulations

Firstly, the simulator must have neural network supportability, i.e., the simulator can load neural networks and perform forward propagation of neural networks.

As for the simultaneous approach, the simulator needs to additionally support backward propagation of neural networks for integrating neural models. Taking the neural DAE module and the implicit trapezoidal method as an example, the algebraic integration function is shown in (31) and the injection currents are calculated as shown in (32). The partial derivatives with respect to the input vector of the neural module are needed, as shown in (33):

$$\mathbf{F}(\mathbf{x}, \mathbf{i}, \mathbf{v}, \mathbf{z}, t) = \mathbf{x}(t) - \left\{ \mathbf{x}(t - \Delta t) + \frac{1}{2} \Delta t \left[ \mathbf{f}_\theta(\mathbf{x}(t), \mathbf{i}(t), \mathbf{v}(t), \mathbf{z}(t); \theta) + \mathbf{f}_\theta(\mathbf{x}(t - \Delta t), \mathbf{i}(t - \Delta t), \mathbf{v}(t - \Delta t), \mathbf{z}(t - \Delta t); \theta) \right] \right\} \quad (31)$$

$$\mathbf{i}(t) = \mathbf{g}_\xi(\mathbf{x}(t), \mathbf{v}(t), \mathbf{z}(t); \xi) \quad (32)$$

$$\begin{bmatrix} \frac{\partial \mathbf{F}}{\partial \mathbf{x}} & \frac{\partial \mathbf{F}}{\partial \mathbf{v}} \\ \frac{\partial \mathbf{G}}{\partial \mathbf{x}} & \frac{\partial \mathbf{G}}{\partial \mathbf{v}} \end{bmatrix} = \begin{bmatrix} \Phi_{11} \left( \frac{\partial \mathbf{f}_\theta}{\partial \mathbf{x}} \right) & \Phi_{12} \left( \frac{\partial \mathbf{f}_\theta}{\partial \mathbf{v}} \right) \\ \Phi_{21} \left( \frac{\partial \mathbf{g}_\xi}{\partial \mathbf{x}} \right) & \Phi_{22} \left( \frac{\partial \mathbf{g}_\xi}{\partial \mathbf{v}} \right) \end{bmatrix} \quad (33)$$

where  $\Phi(*)$  represents a function of  $*$ .

As for the alternating approach, the integration is intuitive. The neural ODE function  $\mathbf{f}_\theta$  is used as the derivative function. It can be easily solved by numerical integration methods such as shown in (8). The neural AE function  $\mathbf{g}_\xi$  is used to calculate injection currents. After adding the calculated injection currents to the connected bus, nodal voltages can be obtained by solving the network AEs (6).

Compared with the DLL files, the neural models can be used in the simultaneous approach as well as in the alternating approach. On the other hand, the integration of neural models will not affect the simulation procedures. In a GPU-based simulator, the calculation of neural networks can be easily implemented and accelerated. Meanwhile, the trained neural models can also be used to analyze

the relativities of input variables and output variables based on the partial derivatives, which can be easily calculated.

### C. Initial Value Learner

For a dynamic component, the initial values of state variables may not be directly accessed, e.g., the initial value of the rotor angle is determined by the nodal voltage and power generation obtained by the power flow solution. It means that  $\mathbf{x}(0)$  may not be directly obtained for the proposed neural modules. Therefore, an initial value learner is needed. In most cases, the learner may be of the form shown in (34).

$$\mathbf{x}(0) = \mathbf{h}_\zeta(\mathbf{i}, \mathbf{v}, \mathbf{z}; \zeta) \quad (34)$$

where  $\mathbf{h}$  is an initial value calculator and  $\zeta$  denotes the parameters.

### D. Discrete Event Handling

During simulations, events such as faults and relay actions will introduce jump changes to the network and operation variables such as nodal voltages. Taking Fig. 2. (b) as an example, the state variable  $\mathbf{x}(t)$  will not change right before and after the event, i.e.,  $\mathbf{x}(t^+) = \mathbf{x}(t^-)$ , whereas some variables in  $\mathbf{z}(t)$  may change, i.e.,  $\mathbf{z}(t^+) \neq \mathbf{z}(t^-)$ . The difference between  $\mathbf{z}(t^+)$  and  $\mathbf{z}(t^-)$  could be large when the power system is subjected to a major failure.

Considering these jump changes during the training process can improve the accuracy of the neural modules. Intuitively, we should use  $\mathbf{z}(t^+)$  instead of  $\mathbf{z}(t^-)$  to predict  $\dot{\mathbf{x}}(t)$ , i.e.,  $\mathbf{z}(t^+)$  should also be sampled in  $\mathcal{S}$ . However, in most power system simulation tools, jump changes cannot be obtained. An acceptable alternative is to use  $\mathbf{z}(t+1)$  instead of  $\mathbf{z}(t)$  to predict  $\dot{\mathbf{x}}(t)$  because the variables at the next integration step are a good approximation of the jump changes. Additional equality constraint (35) is added to (9) and constraints (35), (36), and (37) are added to (18) for discrete event handling:

$$\hat{\mathbf{z}}_i(t^+) = \hat{\mathbf{z}}_i(t+1), t \in \mathbf{T}_{event} \quad (35)$$

$$\hat{\mathbf{v}}_i(t^+) = \hat{\mathbf{v}}_i(t+1), t \in \mathbf{T}_{event} \quad (36)$$

$$\mathbf{i}_i(t^+) = \mathbf{g}_\xi(\mathbf{x}_i(t), \hat{\mathbf{v}}_i(t^+), \hat{\mathbf{z}}_i(t^+); \xi), t \in \mathbf{T}_{event} \quad (37)$$

where  $\mathbf{T}_{event}$  is the set of time instants when events happen. In the simulator, the neural AE function  $\mathbf{g}_\xi$  can be used to calculate the jump changes. The time derivative  $\mathbf{f}_\theta(\mathbf{x}_i(t), \mathbf{i}_i(t^+), \hat{\mathbf{v}}_i(t^+), \hat{\mathbf{z}}_i(t^+); \theta)$  at instant  $t^+$  is used to calculate  $\mathbf{x}_i(t+\Delta t)$ .

### E. Convergence Maintenance

The DAE models trained by the neural DAE modules are connected to the power network as a simple current source of which the current injection can be calculated as shown in (17). However, a current source without a shunt admittance can seriously affect the convergence in most cases, because the network equations may lose diagonal dominance. Therefore, besides the trained DAE model, an additional shunt admittance is also connected to the power network and the injection currents will be recalculated as follows:

$$\mathbf{i}' = \mathbf{i} + \mathbf{v} \cdot (jB') \quad (38)$$

where  $\mathbf{i}'$  is the fictitious injection current and  $B'$  is the fictitious susceptance, which is set to  $-50$  in this paper.

## V. MODULE DESIGNS FOR TYPICAL POWER COMPONENTS

The proposed neural modules can be used to build neural dynamic models for almost any dynamic component in power systems. In this paper, two simple but representative cases are tested to demonstrate the validity and potentiality of the neural modules. The modified neural ODE module is used to model a black-box excitation



TABLE I  
INFORMATION OF NEURAL MODULES AND TRAINING SETTINGS

Models	Structure	Dimensionality	Mini-batch Size & Training Set Size	Learning Rate	Learning Rate Damping Factor	Learning Rate Damping Step & Number of Epoch
<i>Exciter_NE</i>	Fig. 2. (b)	Hidden Layers: 8, 16, 32, 64, <b>128</b>	(1, 50), (2, 100)	0.001,		
<i>Exciter_E</i>	Fig. 2. (c)	Hidden Space: 8, 16, 32, <b>64</b> , 128	(4, 200), (8, 400),	<b>0.005</b> ,	0.5, <b>0.7</b>	(5,50), (10, 100),
<i>Gen_NE</i>	Fig. 2. (d)	Hidden Layers: 8, 16, 32, 64, <b>128</b>	(16, 800), (32, 1600),	0.01		(20, 200), ( <b>40, 400</b> )
<i>Gen_E</i>	Fig. 2. (e)	Hidden Space: 8, 16, 32, <b>64</b> , 128	<b>(64, 3200)</b>			

controller. The neural DAE module is used to model a classic synchronous machine. The trained models are integrated into an alternating approach-based simulator to test the performances of these modules in actual transient simulations.

#### A. Modified Neural ODE Module Designs for a Black-box Exciter

A common excitation controller model displayed in Fig. 3 is used to test the modified neural ODE module. Only the input variables  $V$  and  $V_s$  and the output variable  $E_{fd}$  of the exciter are accessible, i.e., the exciter is a black box for simulations. This is a commonly encountered situation when building controller models based on DLL files. Since the exciter is used as a representative of black-box regulators,  $E_{fd \max}$  and  $E_{fd \min}$  are set to plus and minus infinity, respectively, to test the generalization ability of the models.

Two modified neural ODE modules are implemented. One is the regular module without an autoencoder called *Exciter\_NE*. The other one called *Exciter\_E* utilizes an autoencoder. The input and output settings are shown in (39):

$$\begin{aligned} \mathbf{x}(t) &= \{E_{fd}(t)\} \\ \mathbf{z}(t) &= \{V(t), V_s(t), V(0), V_s(0), \mathbf{x}(0)\} \end{aligned} \quad (39)$$

In  $\mathbf{z}$ , the initial steady-state values of  $V$ ,  $V_s$ , and  $E_{fd}$  are included so that the neural ODE block can learn how to calculate the reference variables  $V_{ref}$  and  $E_{fdref}$ . In most cases,  $V_{ref}$  and  $E_{fdref}$  are unknown and calculated based on the steady state of the exciter. If the reference variables are known, they can be used to form  $\mathbf{z}$ .

#### B. Neural DAE Module Designs for a Synchronous Machine

The classic generator model shown in (40) is the simplest grid-connected dynamic component with state variables and injection current. Therefore, it is selected as the representative to test the performance of neural DAE modules.

$$\begin{cases} T_j \frac{d\omega}{dt} = \frac{P_T - P_E}{\omega} \\ \frac{d\delta}{dt} = (\omega - 1)2\pi f_0 \end{cases} \quad (40)$$

where  $T_j$  is the inertia time constant,  $\omega$  is the per-unit value of the rotation speed,  $\delta$  is the rotor angle,  $P_T$  is the mechanical power,  $P_E$  is the electromagnetic power, and  $f_0$  is the rated frequency.

Two neural DAE modules are implemented. One is the regular module without an autoencoder called *Gen\_NE*. The other one called *Gen\_E* utilizes an autoencoder. The input and output settings are shown in (41).

$$\begin{aligned} \mathbf{x}(t) &= \{\omega(t), \delta(t)\} \\ \mathbf{z}(t) &= \{\mathbf{x}(0), v_x(0), v_y(0), i_x(0), i_y(0)\} \\ \mathbf{v}(t) &= \{v_x(t), v_y(t)\} \\ \mathbf{i}(t) &= \{i_x(t), i_y(t)\} \\ \mathbf{x}(0) &= \mathbf{h}(\mathbf{v}(t), \mathbf{i}(t)) \end{aligned} \quad (41)$$

where  $v_x$  and  $v_y$  are respectively the real part and imaginary part

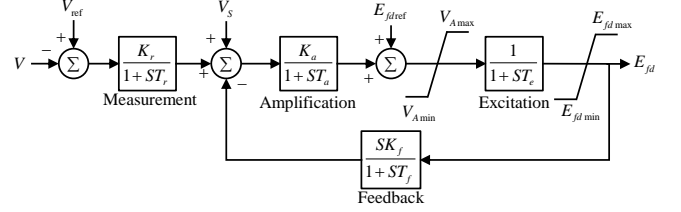


Fig. 3. Excitation system model. The input  $V$  is the amplitude of the nodal voltage. The model contains four blocks including measurement, amplification, excitation, and feedback.  $K$  and  $T$  denote the enlargement factor and the time constant of each block, respectively.  $V_s$  represents the additional input signal from the PSS.  $V_{ref}$  and  $E_{fdref}$  are the reference variables.

of nodal voltage  $\mathbf{v}$ , and  $i_x$  and  $i_y$  are respectively the injection current  $\mathbf{i}$ . The reason for setting the input and output variables as in (41) is that the trained model can be directly integrated into simulations. Besides the neural DAE modules, a neural network  $\mathbf{h}$  with two hidden layers that learns the initial values  $\mathbf{x}(0)$  is also established.

The neural modules will be tested under three different situations. The first one is to train a purely data-driven model without any physical prior knowledge. Only the curves of input and output variables are utilized. The second one is to train a physics-data-integrated model. In this model, the variation of rotor angle is simulated using the actual dynamic derivative function shown in the second equation of (40), which is also intuitive because the time derivative of rotor angles always meets with that equation. In this case, the neural networks are used to calculate the time derivative of the rotation speed  $\omega$ . The last one is a model calibration test. The exact derivative functions are known whereas the parameters  $T_j$  and the transient reactance  $X'_d$  are unknown. In this case, we could register  $T_j$  and  $x'_d$  as learnable parameters in PyTorch [35] and build a neural DAE module. The parameters can be determined by training.

#### C. Building Neural Modules with Neural Networks

The designs of neural modules can be found in TABLE I. In the “Models” column, “NE” stands for no encoding and “E” stands for encoding. In the “Dimensionality” column, the dimensionality of hidden layers in Fig. 2. (b) and Fig. 2. (d) shows the width of the hidden layers. The neural ODE block and the neural AE block are built with a fully connected neural network (FCNN) that contains three hidden layers. All the hidden layers have the same width. The dimensionality of hidden space in Fig. 2. (c) and Fig. 2. (e) shows the dimensionality of the encoded variables. Taking the modified neural module in Fig. 2. (c) as an example, after encoding,  $\mathbf{x}$  and  $\mathbf{z}$  will have the same dimensionality that is equal to the dimensionality of the hidden space. The encoder, decoder, neural ODE block, and neural AE block are all constructed using an FCNN that contains one hidden layer.

In this paper, between any two adjacent neural layers, the exponential linear unit (ELU) [36] is used as the activation function for its good performance. There are no activation functions for

output layers since there is no limit to the output of derivative functions. The L2 norm (27) is used as the loss function. In addition, a gradient clipping technique is adopted to handle the problem of exploding gradient.

## VI. IMPLEMENTATION AND NUMERICAL TESTS

### A. Implementation Overview

The test platform is a Linux server consisting of one Intel i7-10700KF 3.80GHz 8-core CPU, one NVIDIA GeForce RTX 3090 GPU, and 128GB DDR4-3200MHz RAM.

The neural modules are developed with Python based on an open-source neural ODE package called torchdiffeq on GitHub [24]. We also shared our modified neural ODE module and neural DAE module on GitHub ([https://github.com/xxh0523/Py\\_PSNODE](https://github.com/xxh0523/Py_PSNODE)). An alternating approach-based high-performance transient simulator called Power System Optimal Parameter Selection (PSOPS), which is purely written in C++ based on our previous studies [37], [38], and [39], is adopted as the simulator. The PyTorch C++ application programming interface (API) is used in the simulator to enable neural network supportability. It can directly load the structure and parameters of neural networks and perform forward and backward propagations of neural networks. The Python API of the PSOPS simulator called Py\_PSOPS is developed and made public [40].

### B. Training and Testing Designs

The test system is the standard IEEE-39 system. Except for the generator connected to Bus-31, which is modeled by the classic second-order generator model, the other components are modeled in detail including the sixth-order generator model, exciters, governors and movers, power system stabilizers (PSS), and induction motor load models. Power flow can be randomly sampled by changing the generation and load through Py\_PSOPS. Each sampled operating state can be subjected to a random fault or disturbance including three-phase short-circuit and open-circuit faults, generator tripping, load shedding, etc. The simulation time is 10 seconds and the integration step is 0.01 seconds. To ensure the diversity of samples, half of the samples maintain rotor angle stability whereas the other half of the samples lose rotor angle stability.

For each module, a total number of 4000 samples are generated, of which 800 samples are used as the testing set and the rest 3200 samples are used as the training set. The Adam optimizer is adopted to update parameters. Tests are performed with different training settings to check the requirements and performance of each module. The tested training settings can be found in TABLE I. As can be seen, modules with different structures and complexity are trained with different sample numbers, damping learning rates, and numbers of epochs. We firstly run a few tests with the whole training set, the most complex neural modules, and the longest epochs to check the influence of learning rates. All the learning rate settings shown in TABLE I obtain acceptable models. Therefore, we fix the learning rate to 0.005 and the learning rate damping factor to 0.7 in the following tests.

For each module, the training tests are carried out in the following three steps. Firstly, decrease the size of the training set to find out how many samples are required for obtaining a model with acceptable performance. The size of the training set has a direct influence on whether the neural modules can be used for dynamic component modeling in practical power systems. We hope that the modules can cope with training sets of different sizes. Secondly,

TABLE II  
SUGGESTED TRAINING SETTINGS FOR EACH MODULE

Models	Mini-batch Size & Training Set Size	Dimensionality	Learning Rate Damping Step & Number of Epoch
<i>Exciter_NE</i>	(4, 200)	Hidden layers: 64	(5, 50)
<i>Exciter_E</i>	(4, 200)	Hidden space: 16	(40, 400)
<i>Gen_NE</i>	(16, 800)	Hidden layers: 64	(40, 400)
<i>Gen_E</i>	(8, 400)	Hidden space: 32	(20, 200)

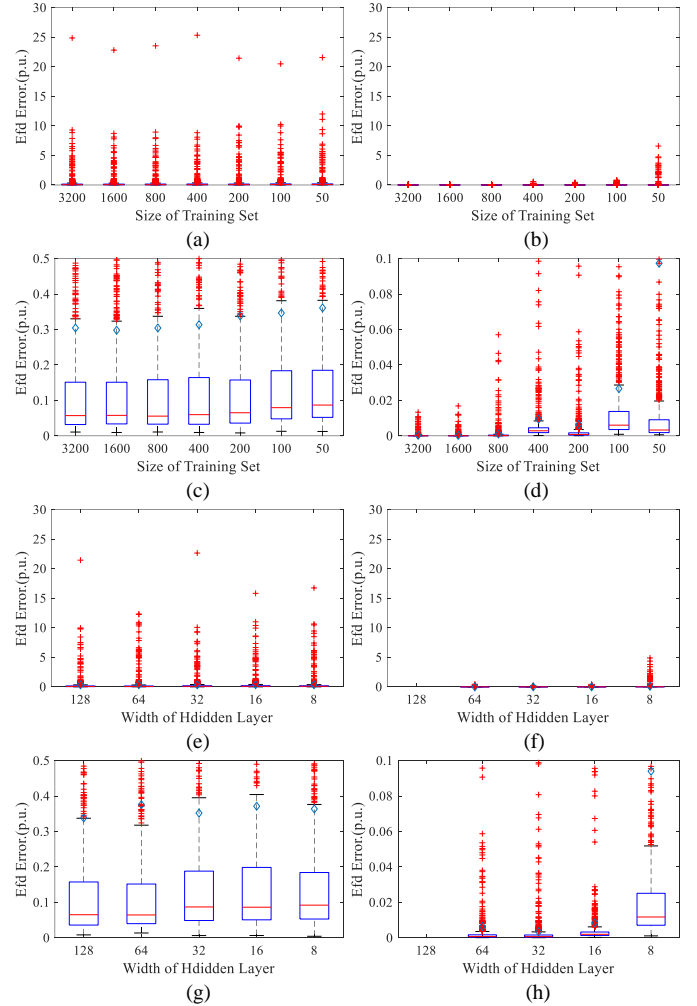


Fig. 4. Box figures of errors of the proposed modified neural ODE modules in the test set of 800 samples. The left column belongs to the Exciter\_NE model and the right column belongs to the Exciter\_E model. The box figures of errors of  $E_{fd}$  with respect to the size of the training set are shown in (a) to (d). The small hollow diamonds denote the mean values. The only difference between (a) and (c) and between (b) and (d) lies in the range of axis y. The errors w.r.t the dimensionality of the modules are displayed in (e) to (h).

decrease the complexity of neural modules, which is the widths of neural layers in this paper. The complexity will affect the execution efficiency of neural module-integrated simulations. At last, decrease the total number of epochs to accelerate the training process. The **bold settings** in TABLE I are chosen as the **baseline** training settings.

After the training tests, the recommended training settings for each module can be found in TABLE II. Then the trained models are tested in actual transient simulations. Detailed test results are as follows.

### C. Testing Details of the Modified Neural ODE Module

#### 1) Tests of Training Settings

Firstly, as mentioned before, we test the sample requirements of

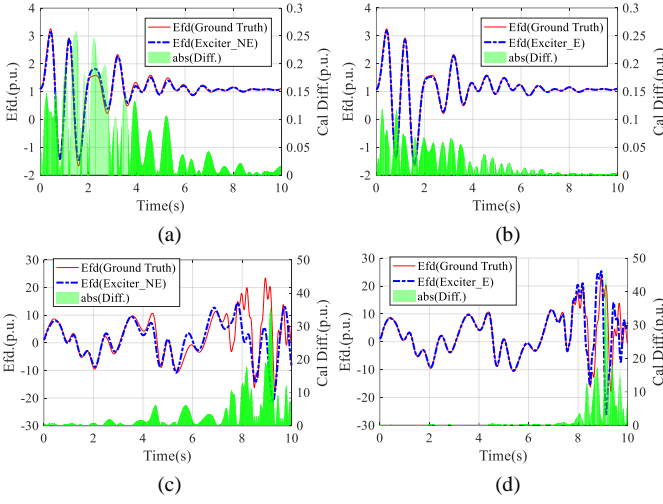


Fig. 5. Output curves of the proposed modified neural ODE models-integrated simulations. The left column belongs to the Exciter\_NE model and the right column belongs to the Exciter\_E model. The solid lines and the dash-dotted lines represent the ground-truth curves and the curves obtained by neural model-integrated simulations, respectively. The results of a stable contingency are displayed in (a) and (b), whereas those of an unstable contingency are shown in (c) and (d). Under the unstable contingency, the system loses rotor angle stability in about 8 seconds.

the proposed modules. Tests results are shown in Fig. 4. (a) to Fig. 4. (d). The box figures illustrate that both Exciter\_NE and Exciter\_E can work normally with training sets of different sizes. The accuracy of the Exciter\_E model outperforms the Exciter\_NE model, which demonstrates the performance improvement due to the autoencoder. As for the Exciter\_NE model, the performance varies little, which indicates that the structural defect of the Exciter\_NE model is causing the relatively low accuracy. We also checked the outliers in the samples. The outliers are all samples with sharp and quick fluctuation in the output. On the other hand, the errors of the Exciter\_E model grow as the size of the training set decreases, which is intuitive.

Secondly, the size of the training set is fixed at 200. We test the neural modules with different dimensionality settings, which are the widths of hidden layers of the neural modules. Testing results are shown in Fig. 4. (e) to Fig. 4. (h). We select 64 for the Exciter\_NE model and 16 for the Exciter\_E model. Notably, the Exciter\_E model is more likely to suffer from exploding gradients. In our tests, when the dimensionality of hidden space is set to 128, as shown in Fig. 4. (f) and Fig. 4. (h), the training process will fail.

Thirdly, the width of hidden layers is also fixed to test the required number of training epochs. Based on the test results, the recommended settings are shown in TABLE II. The number of training epochs affects the performance of the Exciter\_E model more than the Exciter\_NE model, which also implies that the structural defect of the Exciter\_NE model is the main reason for the relatively low accuracy.

Finally, the suggested training settings are shown in TABLE II. With only 200 samples, which is not very difficult to obtain in practical power systems, both modules provide acceptable predictions of the output, which indicates that the proposed modules have the potential for practical application. In particular, the autoencoder-based neural ODE module can provide an extremely accurate approximation of the original dynamics of the component.

## 2) Accuracy of Neural Model-Integrated Simulations

The models obtained under the suggested training settings are integrated into the PSOPS simulator. In Fig. 5. (a) to Fig. 4. (d), the curves of excitation voltage and the errors between the learned

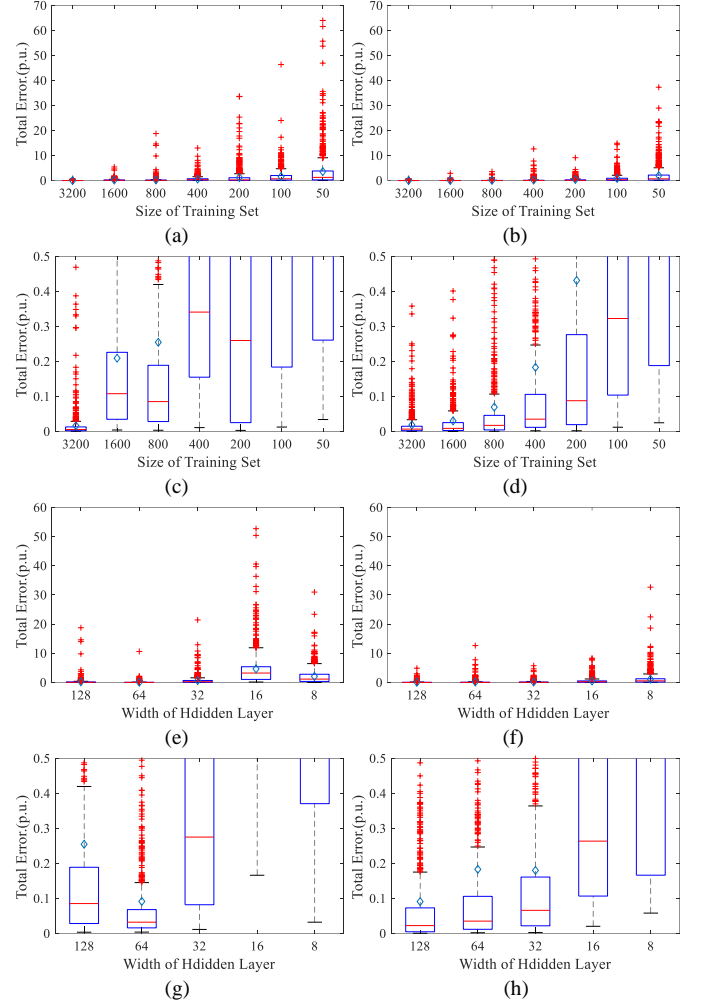


Fig. 6. Box figures of errors of the proposed neural DAE modules in the test set of 800 samples. The displayed error is the total error of  $\mathbf{x}$  and  $\mathbf{i}$ . The left column belongs to the Gen\_NE model and the right column belongs to the Gen\_E model. The box figures of errors w.r.t. the size of the training set are shown in (a) to (d). The small hollow diamonds denote the mean values. The only difference between (a) and (c) and between (b) and (d) lies in the range of axis y. The errors w.r.t. the dimensionality of the modules are displayed in (e) to (h).

model and the original model are displayed. When the system is stable as shown in Fig. 5. (a) and Fig. 5. (b) or before the system loses stability as shown in Fig. 5. (c) and Fig. 5. (d), the models Exciter\_NE and Exciter\_E can both perform well in actual simulations. The Exciter\_E model works better than the Exciter\_NE model with smaller errors. When the system loses stability, both models deviate from the ground truth. However, this deviation is acceptable because the simulation of an unstable state is physically meaningless. As long as the simulation gives an unstable prediction for an unstable contingency, the neural models can be used. It should be noted that the time consumption of neural model-integrated simulations will increase. It is intuitive since the computational burden increases with the number of parameters.

## D. Testing Details of the Neural DAE Module

### 1) Training Requirements

Similar three-step tests of the Gen\_NE model and the Gen\_E model are carried out and the test results are shown in Fig. 6. Notably, the prediction errors are relatively large compared with the exciter. It is reasonable since the number of predicted outputs is four in the generator versus one in the exciter. The performance of the autoencoder-based module is also better and stabler than the regular



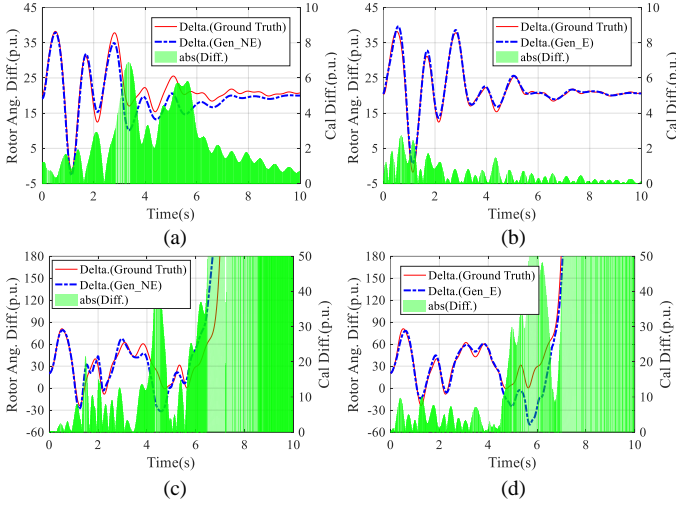


Fig. 7. Curves of the rotor angle difference between the neural model and the generator at BUS-39 of the proposed neural DAE models-integrated simulations. The left column belongs to the Gen\_NE model and the right column belongs to the Gen\_E model. The solid lines and the dash-dotted lines represent the ground-truth curves and the curves obtained by neural model-integrated simulations, respectively. The results of a stable contingency are displayed in (a) and (b), whereas those of an unstable contingency are shown in (c) and (d). Under the unstable contingency, the system loses rotor angle stability in about 7 seconds.

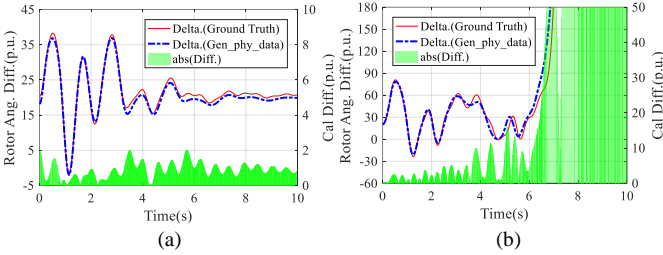


Fig. 8. Output curves of the physics-informed neural DAE models-integrated simulations. The training settings are the same as the suggested settings of the Gen\_NE model shown in TABLE II.

TABLE III  
RESULTS OF MODEL CALIBRATION

Parameter Set	Ground Truth	Learned Value	Errors (%)
1	$(x'_d = 0.0414706,$	$(x'_d = 0.0429254,$	$(x'_d : +3.51\%,$
	$T_j = 50.932)$	$T_j = 50.9739)$	$T_j : +0.08\%)$
2	$(x'_d = 0.0397059,$	$(x'_d = 0.0399874,$	$(x'_d : +0.71\%,$
	$T_j = 28.8932)$	$T_j = 29.3497)$	$T_j : +5.13\%)$
3	$(x'_d = 0.0513235,$	$(x'_d = 0.0508575,$	$(x'_d : -0.91\%,$
	$T_j = 61.2952)$	$T_j = 62.6543)$	$T_j : 2.22\%)$

one. The suggested training settings are also shown in TABLE II.

#### 2) Accuracy of Neural DAE Model-Integrated Simulations

The trained models are integrated into the PSOPS simulator. Tests results can be found in Fig. 7. Compared with the exciter models, learned generator models introduce more errors. The reason is intuitive. The exciter influences only a small part of the connected generator. It cannot directly affect the dynamics of the whole power network. In contrast, a generator model can directly influence the whole network through injection currents. A very small difference in the model may lead to a large difference in the result after numerical integration. Therefore, the errors shown in Fig. 7 are within an acceptable range.

#### 3) Physics-data Integrated Model

The test results are shown in Fig. 8. As can be seen, with the

derivative equation of rotor angle known, the performance of the neural DAE module without autoencoder upgrades.

#### 4) Accuracy of Parameter Estimation

Three sets of parameters are used for the model calibration tests. The results can be found in TABLE III. Since the L2 norm loss function is used, it is essentially a least square regression based on the neural DAE framework and automatic differentiation. The estimated parameters are sufficiently accurate.

## VII. DISCUSSIONS ON FUTURE WORKING DIRECTIONS

### A. Measurement-based Neural Modules

In practical power systems, real-time measurements from phasor measurement units (PMUs) and fault recorders can be used to build dynamic models based on neural ODE [25]. The neural modules proposed in this paper should also work properly with real-time measurements. The challenge is to obtain sufficiently diverse samples. In the samples used in this paper, stable samples and unstable samples each account for half. We also tested the proposed modules with unbalanced samples. Of course, most of the samples are stable. The performance will degrade when facing unstable contingencies. How to accurately generalize the model to precisely approximate the stable boundary is a future working direction.

### B. Equivalent Modeling

Another mentioned but not discussed possible application of the neural modules is the equivalent modeling of stations or networks. Based on detailed modeled stations or networks, an equivalent model based on neural modules can be established. The neural module-based equivalent models could be accurate and might be very helpful for analyzing the dynamic characteristics of renewable generation and active distribution networks.

### C. Electromagnetic Simulation-based Neural Modules

As for the electromagnetic simulations, the modified neural ODE module can be utilized. The challenge lies in the very small integration step. A very small integration step leads to a very large number of total integration steps. The Python-based training process of the proposed neural modules is time-consuming. The time consumption is directly affected by the total number of integration steps. The reason is that the execution speed of loop functions in Python is very slow. For electromagnetic simulations, the training efficiency should be upgraded and the Julia programming language [41] may be one of the solutions. Developing physics-data-integrated models might be another solution.

## VIII. CONCLUSION

In this paper, we propose the general frameworks of a modified neural ODE module and a neural DAE module for power system transient stability simulations. The mathematics of the backward propagation of these modules is deducted. Autoencoder-based structures are proposed to improve the performance of neural modules. The integration of these neural modules into transient simulators is analyzed. The source code of the neural modules has been made public on GitHub.

All the test results show that the proposed modules can be used in a variety of situations including building a dynamic model for a black-box component, physics-data-integrated modeling, estimating parameters, etc., with hundreds of sampled curves, which proves the validity and the great potentiality of the proposed neural modules.

Future works may focus on adapting the proposed modules to

measurement-based situations, building equivalent models for stations and networks, proposing new designs of neural modules, and upgrading the performance of the neural modules.

## REFERENCES

- [1] N. Hatziaargyriou *et al.*, "Definition and Classification of Power System Stability – Revisited amp; Extended," *IEEE Transactions on Power Systems*, vol. 36, no. 4, pp. 3271–3281, Jul. 2021, doi: 10.1109/TPWRS.2020.3041774.
- [2] J. V. Milanovic, K. Yamashita, S. Martínez Villanueva, S. Ž. Djokic, and L. M. Korunović, "International Industry Practice on Power System Load Modeling," *IEEE Transactions on Power Systems*, vol. 28, no. 3, pp. 3038–3046, Aug. 2013, doi: 10.1109/TPWRS.2012.2231969.
- [3] P. Kundur, N. J. Balu, and M. G. Lauby, *Power system stability and control*, vol. 7. McGraw-hill New York, 1994.
- [4] A. Honrubia-Escribano, E. Gómez-Lázaro, J. Fortmann, P. Sørensen, and S. Martín-Martínez, "Generic dynamic wind turbine models for power system stability analysis: A comprehensive review," *Renewable and Sustainable Energy Reviews*, vol. 81, pp. 1939–1952, Jan. 2018, doi: 10.1016/j.rser.2017.06.005.
- [5] S. R. Pendem and S. Mikkili, "Modeling, simulation and performance analysis of solar PV array configurations (Series, Series-Parallel and Honey-Comb) to extract maximum power under Partial Shading Conditions," *Energy Reports*, vol. 4, pp. 274–287, Nov. 2018, doi: 10.1016/j.egyr.2018.03.003.
- [6] R. A. Biroon, P. Pisu, and D. Schoenwald, "Large-Scale Battery Energy Storage System Dynamic Model for Power System Stability Analysis," in *2020 IEEE Texas Power and Energy Conference (TPEC)*, Feb. 2020, pp. 1–5. doi: 10.1109/TPEC48276.2020.9042536.
- [7] J. K. Nøland, E. F. Alves, A. Pardini, and U. Lundin, "Unified Reduced Model for a Dual-Control Scheme of the High-Speed Response Brushless Excitation System of Synchronous Generators," *IEEE Transactions on Industrial Electronics*, vol. 67, no. 6, pp. 4474–4484, Jun. 2020, doi: 10.1109/TIE.2019.2931270.
- [8] S. Mohajeryami, A. R. Neelakantan, I. N. Moghaddam, and Z. Salami, "Modeling of deadband function of governor model and its effect on frequency Response characteristics," in *2015 North American Power Symposium (NAPS)*, Oct. 2015, pp. 1–5. doi: 10.1109/NAPS.2015.7335089.
- [9] A. Khodabakhshian, R. Hemmati, and M. Moazzami, "Multi-band power system stabilizer design by using CPCE algorithm for multi-machine power system," *Electric Power Systems Research*, vol. 101, pp. 36–48, Aug. 2013, doi: 10.1016/j.epsr.2013.03.011.
- [10] A. Arif, Z. Wang, J. Wang, B. Mather, H. Bashualdo, and D. Zhao, "Load Modeling—A Review," *IEEE Transactions on Smart Grid*, vol. 9, no. 6, pp. 5986–5999, Nov. 2018, doi: 10.1109/TSG.2017.2700436.
- [11] S. Guo, S. Norris, and J. Bialek, "Adaptive Parameter Estimation of Power System Dynamic Model Using Modal Information," *IEEE Transactions on Power Systems*, vol. 29, no. 6, pp. 2854–2861, Nov. 2014, doi: 10.1109/TPWRS.2014.2316916.
- [12] F. Ding, J. Pan, A. Alsaedi, and T. Hayat, "Gradient-Based Iterative Parameter Estimation Algorithms for Dynamical Systems from Observation Data," *Mathematics*, vol. 7, no. 5, Art. no. 5, May 2019, doi: 10.3390/math7050428.
- [13] P. Ju, C. Qin, F. Wu, H. Xie, and Y. Ning, "Load modeling for wide area power system," *International Journal of Electrical Power & Energy Systems*, vol. 33, no. 4, pp. 909–917, May 2011, doi: 10.1016/j.ijepes.2010.12.030.
- [14] E. Acilan and M. Gol, "Identifiability Analysis for Power Plant Parameter Calibration in the Presence of Collinear Parameters," *IEEE Transactions on Power Systems*, pp. 1–1, 2021, doi: 10.1109/TPWRS.2021.3130076.
- [15] B. Yang *et al.*, "Comprehensive overview of meta-heuristic algorithm applications on PV cell parameter identification," *Energy Conversion and Management*, vol. 208, p. 112595, Mar. 2020, doi: 10.1016/j.enconman.2020.112595.
- [16] R. Huang *et al.*, "Calibrating Parameters of Power System Stability Models Using Advanced Ensemble Kalman Filter," *IEEE Transactions on Power Systems*, vol. 33, no. 3, pp. 2895–2905, May 2018, doi: 10.1109/TPWRS.2017.2760163.
- [17] R. Fan, R. Huang, and R. Diao, "Gaussian Mixture Model-Based Ensemble Kalman Filter for Machine Parameter Calibration," *IEEE Transactions on Energy Conversion*, vol. 33, no. 3, pp. 1597–1599, Sep. 2018, doi: 10.1109/TEC.2018.2849856.
- [18] S. R. Khazeiynasab and J. Qi, "Generator Parameter Calibration by Adaptive Approximate Bayesian Computation With Sequential Monte Carlo Sampler," *IEEE Transactions on Smart Grid*, vol. 12, no. 5, pp. 4327–4338, Sep. 2021, doi: 10.1109/TSG.2021.3077734.
- [19] R. Nagi, X. Huan, and C. Chen, "Bayesian Inference of Parameters in Power System Dynamic Models Using Trajectory Sensitivities," *IEEE Transactions on Power Systems*, pp. 1–1, 2021, doi: 10.1109/TPWRS.2021.3104536.
- [20] S. Wang, R. Diao, C. Xu, D. Shi, and Z. Wang, "On Multi-Event Co-Calibration of Dynamic Model Parameters Using Soft Actor-Critic," *IEEE Transactions on Power Systems*, vol. 36, no. 1, pp. 521–524, Jan. 2021, doi: 10.1109/TPWRS.2020.3030164.
- [21] A. M. Azmy, I. Erlich, and P. Sowa, "Artificial neural network-based dynamic equivalents for distribution systems containing active sources," *IEEE Proceedings - Generation, Transmission and Distribution*, vol. 151, no. 6, pp. 681–688, Nov. 2004, doi: 10.1049/ip-gtd:20041070.
- [22] S. rashid R. Khazeiynasab, J. Zhao, I. Batarseh, and B. Tan, "Power Plant Model Parameter Calibration Using Conditional Variational Autoencoder," *IEEE Transactions on Power Systems*, pp. 1–1, 2021, doi: 10.1109/TPWRS.2021.3107515.
- [23] B. Lusch, J. N. Kutz, and S. L. Brunton, "Deep learning for universal linear embeddings of nonlinear dynamics," *Nature Communications*, vol. 9, no. 1, Art. no. 1, Nov. 2018, doi: 10.1038/s41467-018-07210-0.
- [24] R. T. Q. Chen, Y. Rubanova, J. Bettencourt, and D. K. Duvenaud, "Neural Ordinary Differential Equations," *Advances in Neural Information Processing Systems*, vol. 31, pp. 6571–6583, 2018.
- [25] P. Zhang and Y. Zhou, "Neuro-Reachability of Networked Microgrids," *IEEE Transactions on Power Systems*, pp. 1–1, 2021, doi: 10.1109/TPWRS.2021.3085706.
- [26] Z. Li *et al.*, "Fourier Neural Operator for Parametric Partial Differential Equations," *arXiv:2010.08895 [cs, math]*, Oct. 2020, Accessed: Nov. 05, 2020. [Online]. Available: <http://arxiv.org/abs/2010.08895>
- [27] M. Mattheakis, D. Sondak, A. S. Dogra, and P. Protopapas, "Hamiltonian Neural Networks for solving differential equations," *arXiv:2001.11107 [physics]*, Feb. 2020, Accessed: Aug. 14, 2021. [Online]. Available: <http://arxiv.org/abs/2001.11107>
- [28] M. Cranmer, S. Greydanus, S. Hoyer, P. Battaglia, D. Spergel, and S. Ho, "Lagrangian Neural Networks," *arXiv:2003.04630 [physics, stat]*, Jul. 2020, Accessed: Aug. 14, 2021. [Online]. Available: <http://arxiv.org/abs/2003.04630>
- [29] L. S. Pontryagin, *Mathematical Theory of Optimal Processes*, 1st ed. Routledge, 1962. doi: 10.1201/9780203749319.
- [30] M. Benning, E. Celledoni, M. J. Ehrhardt, B. Owren, and C.-B. Schönlieb, "Deep learning as optimal control problems: models and numerical methods," *arXiv:1904.05657 [cs, math]*, Sep. 2019, Accessed: Nov. 13, 2020. [Online]. Available: <http://arxiv.org/abs/1904.05657>
- [31] D. P. Kingma and J. Ba, "Adam: A Method for Stochastic Optimization," *arXiv:1412.6980 [cs]*, Jan. 2017, Accessed: Dec. 09, 2020. [Online]. Available: <http://arxiv.org/abs/1412.6980>
- [32] K. He, X. Chen, S. Xie, Y. Li, P. Dollár, and R. Girshick, "Masked Autoencoders Are Scalable Vision Learners," *arXiv:2111.06377 [cs]*, Nov. 2021, Accessed: Nov. 27, 2021. [Online]. Available: <http://arxiv.org/abs/2111.06377>
- [33] S. Dasgupta and A. Gupta, "An elementary proof of the Johnson-Lindenstrauss Lemma," 1999.
- [34] H. W. Dommel and N. Sato, "Fast Transient Stability Solutions," *IEEE Transactions on Power Apparatus and Systems*, vol. PAS-91, no. 4, pp. 1643–1650, Jul. 1972, doi: 10.1109/TPAS.1972.293341.
- [35] "PyTorch," <https://pytorch.org/>
- [36] D.-A. Clevert, T. Unterthiner, and S. Hochreiter, "Fast and Accurate Deep Network Learning by Exponential Linear Units (ELUs)," *arXiv:1511.07289 [cs]*, Feb. 2016, Accessed: Nov. 14, 2021. [Online]. Available: <http://arxiv.org/abs/1511.07289>
- [37] T. Xiao, J. Wang, Y. Gao, and D. Gan, "Improved Sparsity Techniques for Solving Network Equations in Transient Stability Simulations," *IEEE Trans. Power Syst.*, vol. 33, no. 5, pp. 4878–4888, Sep. 2018, doi: 10.1109/TPWRS.2018.2803200.
- [38] T. Xiao, W. Tong, and J. Wang, "A New Fully Parallel BBDF Method in Transient Stability Simulations," *IEEE Trans. Power Syst.*, vol. 35, no. 1, pp. 304–314, Jan. 2020, doi: 10.1109/TPWRS.2019.2933637.
- [39] T. Xiao, W. Tong, and J. Wang, "Study on Reducing the Parallel Overhead of the BBDF Method for Power System Transient Stability Simulations," *IEEE Trans. Power Syst.*, vol. 35, no. 1, pp. 539–550, Jan. 2020, doi: 10.1109/TPWRS.2019.2929775.
- [40] T. Xiao, Y. Chen, J. Wang, S. Huang, W. Tong, and T. He, "Exploration of AI-Oriented Power System Transient Stability Simulations," *arXiv:2110.00931 [cs, eess]*, Oct. 2021, Accessed: Oct. 24, 2021. [Online]. Available: <http://arxiv.org/abs/2110.00931>
- [41] M. Innes *et al.*, "A Differentiable Programming System to Bridge Machine Learning and Scientific Computing," Jul. 2019, Accessed: Feb. 01, 2021. [Online]. Available: <https://arxiv.org/abs/1907.07587v2>